View metadata, citation and similar papers at core.ac.uk
brought to you by CORE
provided by NASA Technical Reports Server

IX. Polymer Research

PROPULSION DIVISION

A. Estimation of Solubility Parameters From Refractive Index Data, *D. D. Lawson and J. D. Ingham*

1. Introduction

For the evaluation of polymeric materials for propellant expulsion bladders, it is often desirable to have a quick and convenient method for estimating solubility parameters. The solubility parameter, or cohesive energy density, of a substance is an extremely fundamental physical constant. Inasmuch as it is a measure of intramolecular forces, it defines many characteristics besides mere solubility. In the case of cryogenic expulsion bladder materials, solubility parameters can be useful in the estimation of glass temperatures (T_g), and also may be used in the study of diffusion processes in elastomers (Refs. 1 and 2). It was suggested by J. Hildebrand and R. Scott (Ref. 3), and later by G. Scatchard (Ref. 4), that solubility parameters could be calculated from optical data such as refractive index measurements. In this article, some semi-empirical correlations between solubility parameters and refractive indices for a series of model compounds and polymers will be discussed.

2. Solubility Parameter Relationships

The potential energy of a mole of material (E) is $E = N_v$, where N is Avogadro's number and the potential energy of a molecule is ν. The cohesive-energy density is thus numerically equal to the negative potential energy of one cubic centimeter of the material ($-E/V$) where V is the molar volume. When solute–solvent systems are to be studied it is convenient to define the square root of the cohesive-energy density as the solubility parameter (δ).

$$\delta^2 = -\frac{E}{V} = -\frac{N\nu}{V} \tag{1}$$

The vaporization of a material can be imagined as a process involving the transport of all molecules from their equilibrium distance, where they have an equilibrium cohesive-energy density, to an effectively infinite distance relative to each other so that the potential energy of each molecule is reduced to zero. The heat of vaporization per mole (Hv) is thus the term used to compensate both for the potential energy per mole (E) and for the volume

work, which for a vapor phase obeying ideal gas laws is RT (where R is the molar gas constant and T is the absolute temperature). That is, $\Delta Hv = -E + RT$. It follows that the cohesive-energy density can then be obtained from Hv and V.

$$\delta^2 = \frac{Hv - RT}{V} \tag{2}$$

This is only true for materials that can be vaporized. In the case of polymers, other means can be used to reliably evaluate $-E/V$. In 1910, P. Walden (Ref. 5) derived an empirical relationship that relates the latent heat of vaporization to refractive index (n). This relationship is

$$lH \cong \frac{310}{M}\left(\frac{n^2 - 1}{n^2 + 2} V\right) \tag{3}$$

where lH is the latent heat of vaporization in cal/g and M is the molecular weight of the material being vaporized. This then can be rewritten so that

$$\Delta Hv \cong 310\left(\frac{n^2 - 1}{n^2 + 2} V\right) \tag{4}$$

Then, by substitution in Eq. (2),

$$\delta \cong \left[310\left(\frac{n^2 - 1}{n^2 + 2}\right) - \frac{RT}{V}\right]^{1/2} \tag{5}$$

By inspection of some data for many model compounds, it was obvious that each chemical class has a value somewhat different from 310. Using these compounds, a series of constants (C) were calculated from

$$C = \frac{Hv}{\left(\frac{n^2 - 1}{n^2 + 2} V\right)} \tag{6}$$

Equation (5) can then be changed to the more general form

$$\delta \cong \left[C\left(\frac{n^2 - 1}{n^2 + 2}\right) - \frac{RT}{V}\right]^{1/2} \tag{7}$$

Table 1 gives average values of C for seven different chemical classes using 57 model compounds. The average value for all 57 compounds is 304.5 which is remarkably close to that of 310 obtained by Walden.

Table 1. Values of C for different chemical types

Chemical type	C calculated from Eq. (6)	Number of materials of each type	Comments and data source
Normal aliphatic hydrocarbons	254.1 ± 2.1	10	This includes 4 alkenes (Refs. 7, 8, 13)
Branched aliphatic hydrocarbons	230.9 ± 9.3	6	Straight chain with methyl groups (Refs. 7, 8, 13)
Aliphatic ethers	279.2 ± 25.0	4	Refs. 7, 8, 13
Aliphatic esters	353.3 ± 30.9	6	Refs. 7, 8, 13
Normal Aliphatic fluoro-carbons	205.1 ± 9.5	4	Refs. 7, 11
Chloro-carbons	330.8 ± 53.1	12	3 methane derivatives and the chloroethanes and chloroethenes (Refs. 7, 12)
Aromatics	287.6 ± 10.4	15	2 aromatic fluorocarbons and 3 cycloalkane +3 cycloalkenes (Refs. 7, 8, 13)

3. Direct Estimation of the Solubility Parameter From Refractive Index Data

The simplest correlation of refractive index and δ is that obtained by a least-square curve fit of the δ of selected organic compounds and the Lorentz–Lorenz function (Ref. 6). By use of 18 compounds, a straight-line fit was obtained that passed through the origin and had a slope of 30.3. The corresponding point-slope-intercept equation is

$$\delta \cong 30.3\left(\frac{n^2 - 1}{n^2 + 2}\right) \tag{8}$$

In Eq. (7), the RT term is of the order of $\sim$600 cal and small when compared to the Hv term ($<10\%$). Thus, the second term can be dropped to give

$$\delta \cong \left[C\frac{n^2 - 1}{n^2 + 2}\right]^{1/2} \tag{9}$$

Equations (8) and (9) permit estimation of solubility parameters from refractive indices.

4. Solubility Parameters of Polymers Calculated From Refractive Index Data

Table 2 shows results for several polymers. The δ were calculated from Eqs. (8) and (9). It can be seen that δ from Eq. (8) do not agree very well with the literature values, but that Eq. (9) gives very reasonable values of δ. Since the second term of Eq. (7) is subtractive, a refined form of Eq. (9) could include a negative constant of the order of a few tenths of a cal/cm^3; however, the effect would be to increase the deviation from other δ values for a few polymers. A relatively arbitrary value of C used for the acrylates (304.5) was the average of the values of Table 1. This value was used primarily because the value determined from aliphatic esters did not result in as good an agreement. It can be concluded that Eq. (9) can be used to obtain satisfactory values of δ from the refractive index for most polymers if a reasonable estimate of C is available.

Table 2. Solubility parameters (δ) estimated from refractive index data

Polymer	Refractive index	δ^a, cal/cm^3	C value used	δ^b, cal/cm^3	δ, cal/cm^3 literature values
Poly(ethylene)	1.51	9.06	254.1	8.72	7.87–8.10 (Ref. 10)
Poly(isobutylene)	1.5089	9.04	230.9	8.31	7.80–8.05 (Ref. 7)
Natural rubber	1.5191	9.20	230.9	8.37	7.90–8.35 (Ref. 10)
Poly(butadiene)	1.5160	9.15	230.9	8.35	8.32–8.60 (Ref. 10)
Poly(styrene)	1.595	10.29	287.6	9.89	8.56–9.70 (Ref. 10)
Poly(methyl acrylate)	1.4725	8.50	304.5	9.24	9.8–10.4 (Ref. 7)
Poly(ethyl acrylate)			304.5	9.44	9.2–9.70 (Ref. 7)
Poly(propyl acrylate)			304.5	9.14	9.0–9.05 (Ref. 7)
Poly(butyl acrylate)			304.5	9.14	8.50–9.10 (Ref. 7)
Poly(vinylidene chloride)	1.63	10.78	330.8	10.39	12.2 (Ref. 7)
Poly(tetrafluoroethylene)	1.35	6.52	205.1	6.49	6.2 (Ref. 10)
Nitroso rubber	1.3170	5.96	205.1	6.36	5.2 (Ref. 9)

[a]Calculated from $\delta = 30.3\ [(n^2 - 1)/(n^2 + 2)]$.

[b]Calculated from $\delta = \{C[n^2 - 1)/(n^2 + 2)]\}^{1/2}$; the δ values for which refractive indices are not given were obtained from calculated molar refractivities divided by specific volumes given in Ref. 6.

References

1. Hayer, R. A., *J. App. Polymer Sci.*, Vol. 15, p. 318, 1961.
2. Van Amerongen, G. J., *Rubber Rev.*, Vol. 37, p. 1092, 1964.
3. Hildebrand, J., and Scott, R., *The Solubility of Nonelectrolytes*, Rheinhold Publishing Corporation, New York, 1948.
4. Scatchard, G., *Chem. Rev.*, Vol. 44, p. 24, 1949.
5. Walden, P., Z. *Phys. Chem.*, Vol. 70, p. 587, 1910.
6. Sewell, J. H., RAE TR 66185, Ministry of Aviation, Farnborough Harts, England, June, 1966.
7. Burrell, H., and Immergut, B., *Polymer Handbook*, Part IV, p. 341, Interscience Publishers division of John Wiley & Sons, Inc., New York, 1966.
8. Riddick, J. A., and Toaps, E. E., *Technique of Organic Chemistry: Volume VII. Organic Solvents*, pp. 43–258, Interscience Publishers division of John Wiley & Sons, Inc., New York, 1955.
9. Crawford, G. H., Rice, D. E., and Sandrum, B. F., *J. Polymer Sci.*, Part A-1, p. 565, 1963.
10. Sheeham C. J., and Bisio, A. L., *Rub. Chem. Tech.*, Vol. 149, 1966.
11. Lovelace, A. M., Rausch, D. A., and Postelnek, W., *Aliphatic Fluorine Compounds*, ACS Monograph Series No. 138, 1958.
12. Huntress, E. H., *Organic Chlorine Compounds*, John Wiley & Sons, New York, 1948.
13. Huntress, E. H., and Mulliken, S. P., *Identification of Pure Organic Compounds*, John Wiley & Sons, New York, 1941.

B. Cationic Crosslinking Agents—Potential Solid Propellant Binders, *A. Rembaum, A. M. Hermann, and H. Keyzer*

1. Introduction

The compounds formed by means of the reaction between an α-ω-dihaloalkane and a tertiary amine containing a double bond yield tetrafunctional monomers (SPS 37-50, Vol. III, pp. 161–165). The latter have positive nitrogens in their structure and therefore may be classified as cationic crosslinking agents. Viscoelastic materials are formed at room temperature with high molecular weight α-ω-dihaloalkanes. This process occurs equally well in presence of large amounts of oxidizers. These materials, characterized by a glass transition temperature of about $-80°C$, show promise as solid propellant binders since they form rubbery products containing positively charged nitrogen atoms.

Low molecular weight α-ω-dihaloalkanes serve as model compounds and are examined here. The investigations

of the viscoelastic materials of more direct interest will be described at a later date.

The synthesis and some characterization details including preliminary nuclear magnetic resonance (NMR) data of cationic crosslinking agents were discussed in SPS 37-50, Vol. III. The present article contains additional analytical NMR results as well as an electron spin resonance (ESR) study of cobalt γ-irradiated crosslinking agents. The radicals obtained during irradiation were identified by means of ESR and the high stability of these materials under the influence of cobalt γ radiation was established.

The irradiation of cationic crosslinking agents in the solid state by means of the cobalt γ source yields a crosslinked polymer, the conversion of monomer to polymer increasing with the radiation dose. The free radical concentration is found to increase initially with the radiation dose, but, in contrast with the percent conversion, it decays rather sharply after reaching a maximum at a dose of about 24 Mrad. The ESR spectra obtained during polymerization under irradiation were found to be identical to those of the crosslinked material formed by polymerization of the monomer using sodium bisulfite and ammonium persulfate as initiator. Thus, the radicals formed during irradiation of monomer are the same as those observed in the irradiation of polymer.

The ESR spectra of methacrylate and acrylate crosslinking agents were very similar to those previously discussed (SPS 37-50, Vol. III) for irradiated methacrylate and acrylate polymers of different structure. This permits a conclusive identification of radicals presently observed.

The crosslinking agent containing an allyl group also yielded an ESR spectrum (after a dose of 50 Mrad) in spite of the fact that no polymerization occurred. This is consistent with the well known general behavior of allyl monomers and with the type of radical identified by means of ESR. In order to gain some insight into the nature of radical disappearance during irradiation, the rate of decay was studied as a function of temperature.

2. Experimental

The NMR spectra were taken at room temperature using the Varian A60 spectrometer. The ESR spectra were taken with the Varian 4502 spectrometer (X band) using 100-kHz modulation. Irradiation doses at room temperature (for the identification of the hyperfine spectra and decay kinetics) were of the order of 2 Mrad; the samples were transferred into quartz tubes after irradiation in pyrex containers.

3. Results

a. NMR analysis. The NMR spectra of a series of crosslinking agents prepared from dimethylaminoethyl acrylate (DA) and methacrylate (DMA) are shown in Fig. 1. The bromine analysis (SPS 37-50, Vol. III) and the good agreement between the integrated intensity of proton absorption (Fig. 1) confirms the postulated structures. It should be noted that the reaction between dibromomethane and DMA leads to a difunctional compound containing a non-ionic bromine atom (Fig. 1f). In this case, only one molecule of DMA reacts because the formation of a cationic crosslinking agent would require presence of two quaternary nitrogens separated by only one CH_2 group. The repulsive interaction of ionic charges is evidently responsible for the formation of a difunctional instead of a tetrafunctional compound. Diallyl crosslinking agents were prepared by a modification of the previous method (SPS 37-50, Vol. III). Allyl bromide was reacted with tetramethylaminoethane and tetramethylaminohexane. The bromine analysis (44.6 and 38.6% theoretical, and 44.3 and 38.3% actual, respectively), as well as the proton integration of the NMR spectra, was found to be in excellent agreement with the theoretical structures (Fig. 2).

b. ESR data. Figure 3 shows the percent conversion and the corresponding ESR intensity with irradiation dose. Figure 4 records the solid state ESR spectra and structure of cationic crosslinking agents. Figure 5 shows the first-order decay of the ESR signal of the dimethacrylate compound (see structure in Fig. 1a) at room temperature. The rate constant calculated from the slope of the figure is 4.8×10^{-4} s^{-1}. A similar study was carried out at 110°C both in air and in vacuum. In both cases, the decay was more rapid than at room temperature and obeyed second-order kinetics (Fig. 6).

The solution of the standard second-order differential equation describing such decay can be cast into the form (Ref. 1)

$$\log\left(1 - \frac{a-b}{N_s}\right) = \frac{b-a}{2.303}\,kt + \log\frac{b}{a}$$

where N_s represents the concentration of unpaired spins at any time t, a is the initial concentration of unpaired spins, b is the initial concentration of the other reactant (presumably oxygen), and k is the rate constant. The

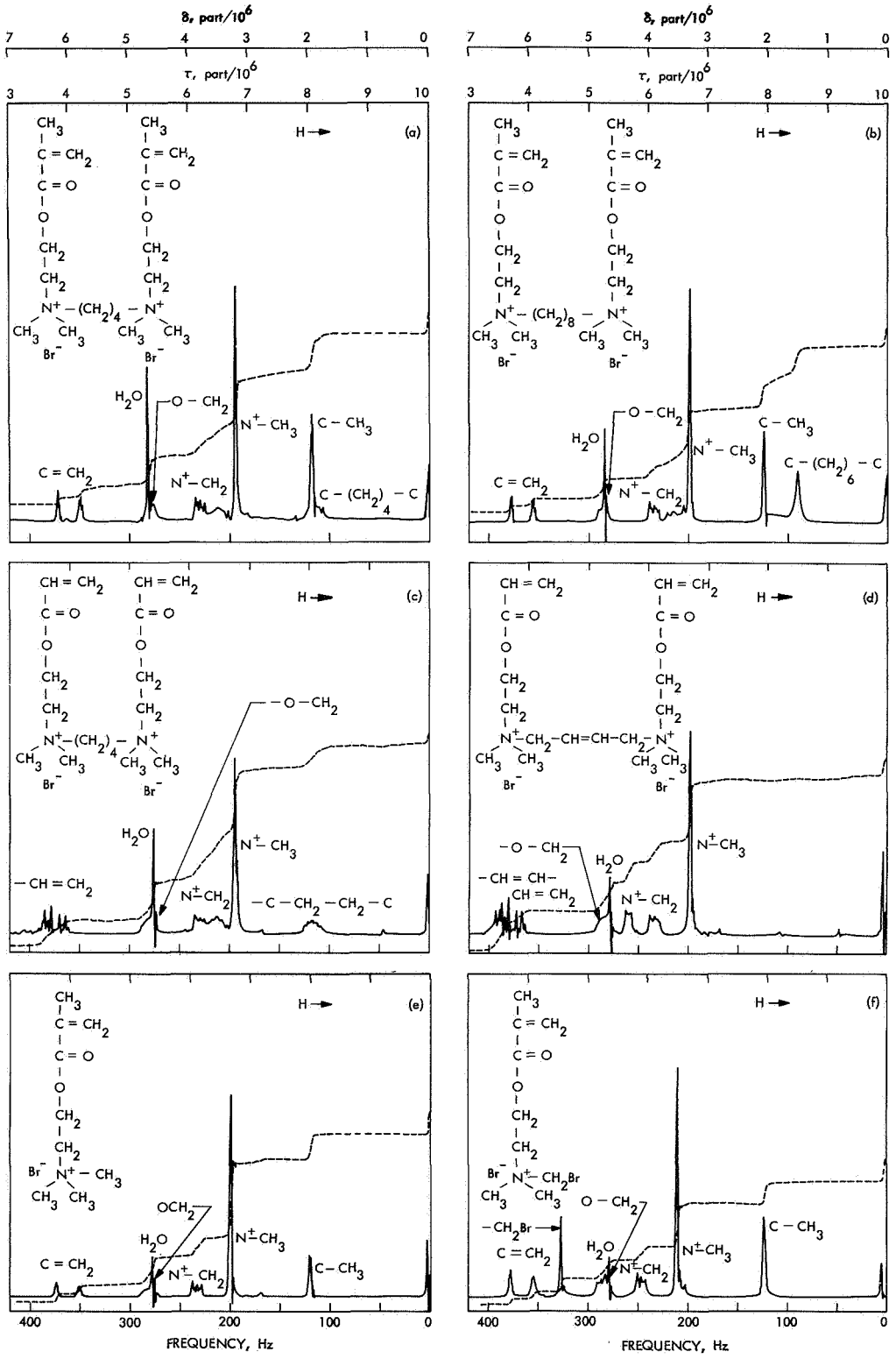

Fig. 1. NMR spectra of methacrylate and acrylate crosslinking agents

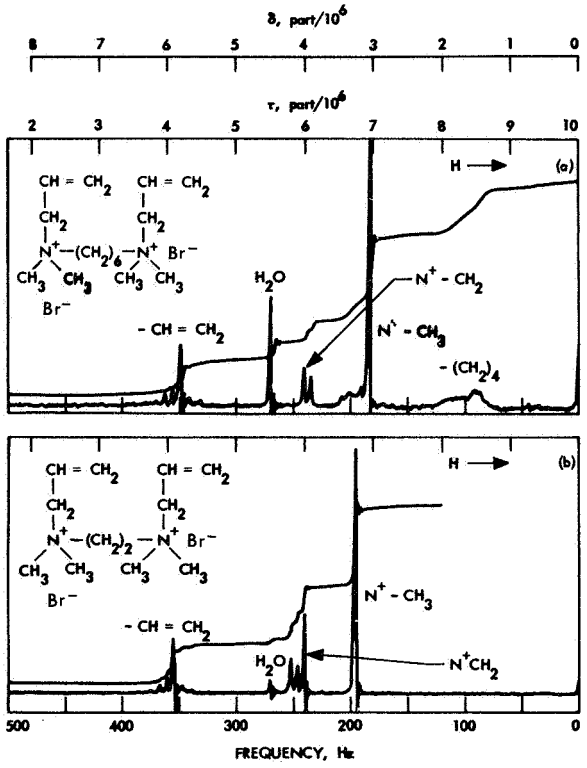

Fig. 2. NMR spectra of allyl crosslinking agents

values of a, N_s, and t are easily measurable. That value of b is chosen to give the best straight line fit on a semi-log plot of $[1 - (a - b)/N_s]$ versus t. In the case of the open-to-air ESR tube (Fig. 6, case A), the value of b required for a straight-line fit is greater than that of a (consistent with excess oxygen), and hence the positive slope. In the case of the evacuated ESR tube (Fig. 6, case B), the value of b required for a straight-line plot is less than that of a (consistent with excess free radicals), and hence the negative slope. Furthermore, it should be mentioned that the rate constant for case A, 128 liters mole^{-1} s^{-1}, is far greater than case B, 3.8 liters mole^{-1} s^{-1}. In terms of raw data, in 1 hr the ESR signal decays to about 2% of its initial value in case A, and to about 50% of its initial value in case B.

4. Discussion

a. ESR spectrum of a methacrylate crosslinking agent. The principal features of the ESR spectrum (see structure in Fig. 1a) are five major lines of approximate intensity ratios 1:4:6:4:1, each line separated from the next by 23.5 G (Fig. 4a). Also observable are two smaller peaks on either side of the central line. While the five major hyperfine lines would suggest interaction with four equivalent protons, one must have further evidence to

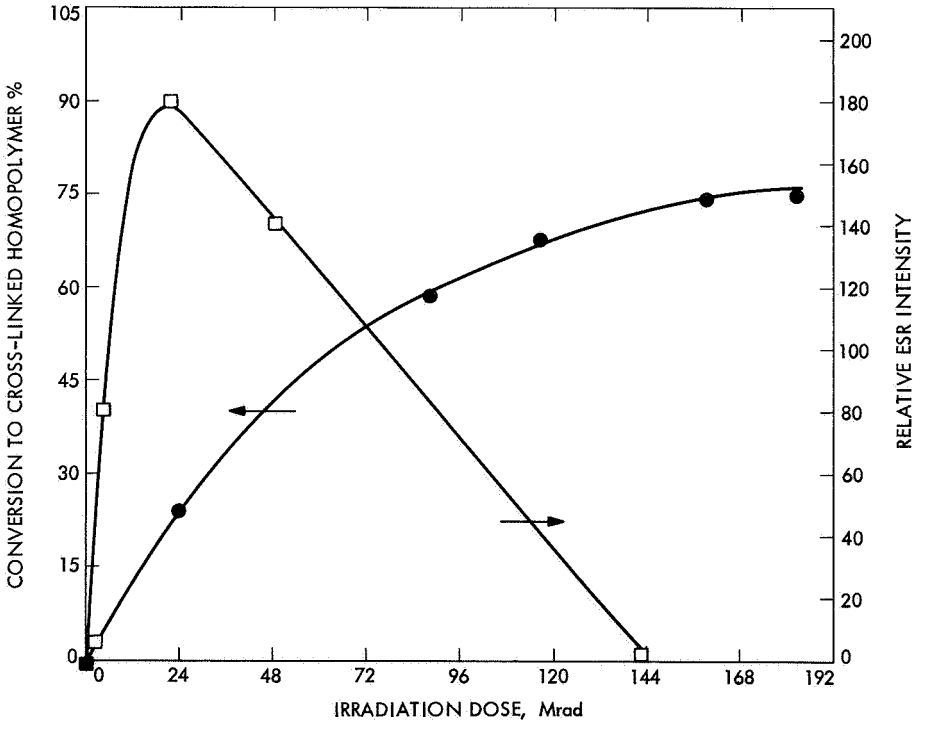

Fig. 3. Percent conversion and relative ESR intensity as a function of γ-irradiation dose for a crosslinking agent (Structure Fig. 1a)

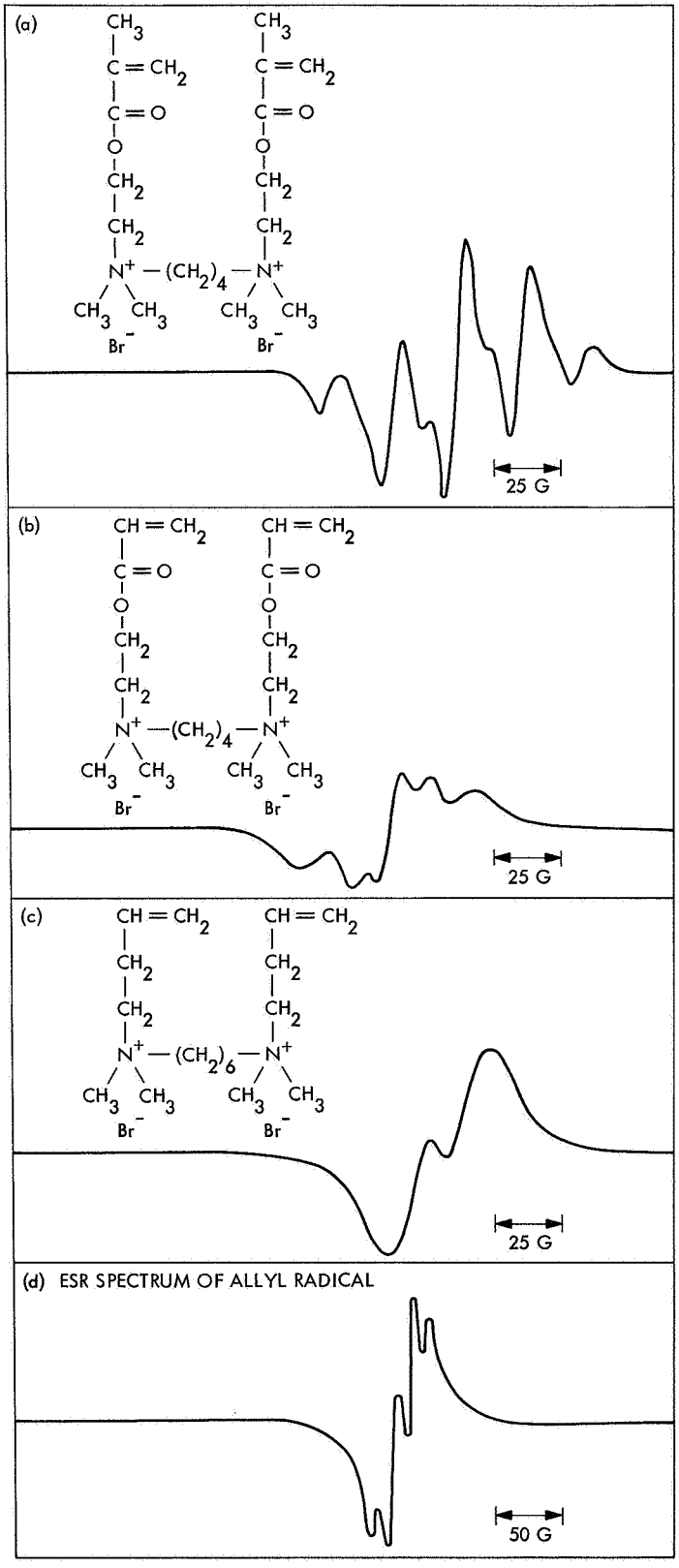

Fig. 4. ESR spectra of γ-irradiated crosslinking agents

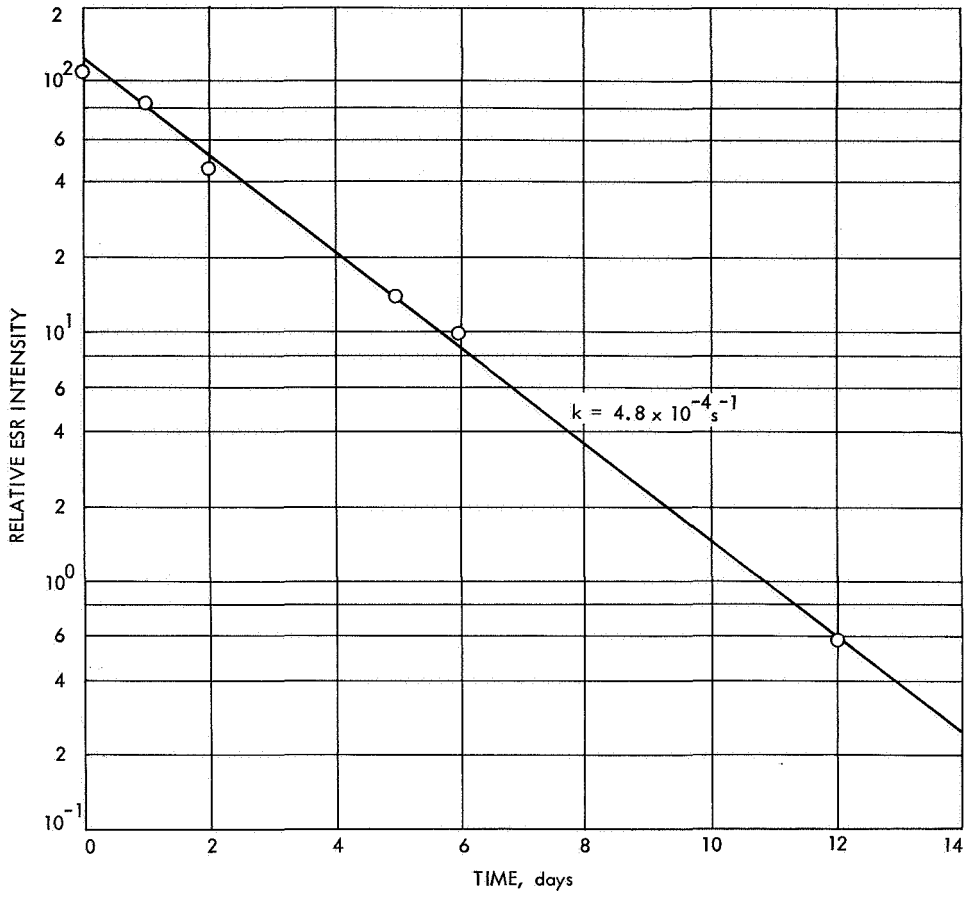

Fig. 5. First-order decay of γ-irradiated crosslinking agents (Structure Fig. 1a)

correctly interpret the unresolved structure. A nearly identical spectrum of irradiated solid methacrylic acid has been reported by H. Fischer (Ref. 2). Fischer has also reported the spectrum of the polymerization radicals of methacrylic acid taken in aqueous solution, thereby affording excellent resolution of each of 16 hyperfine lines giving conclusive evidence for the radical identification. On the basis of Fischer's studies, as well as those of M. C. R. Symons (Ref. 3), the radical whose ESR spectrum is shown (Fig. 4a) is identified as

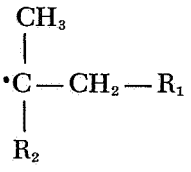

Therefore, it is identical to the radicals previously detected during free radical polymerization of methacrylic monomers.

b. ESR spectrum of an acrylate crosslinking agent. The principal features of the spectrum (see structure in Fig. 1b) are three lines of approximate intensity ratios 1:2:1 separated by about 28 G (Fig. 4b). In addition, there are two other resolved lines on either side of the central peak. This spectrum appears quite similar to that found by R. J. Abraham and D. H. Whiffen (Ref. 4) for γ-irradiated solid polyacrylic acid. On this basis, the radical is identified as

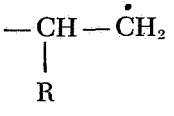

c. ESR spectrum of an allyl crosslinking agent. The principal feature of the spectrum (see structure in Fig. 1c) appears to be two equally intense lines of 21-G separation, but previous evidence suggests this to be superposition of at least four lines (Ref. 5). On the basis of previous studies of the allyl radical (Ref. 5 and Fig. 4d),

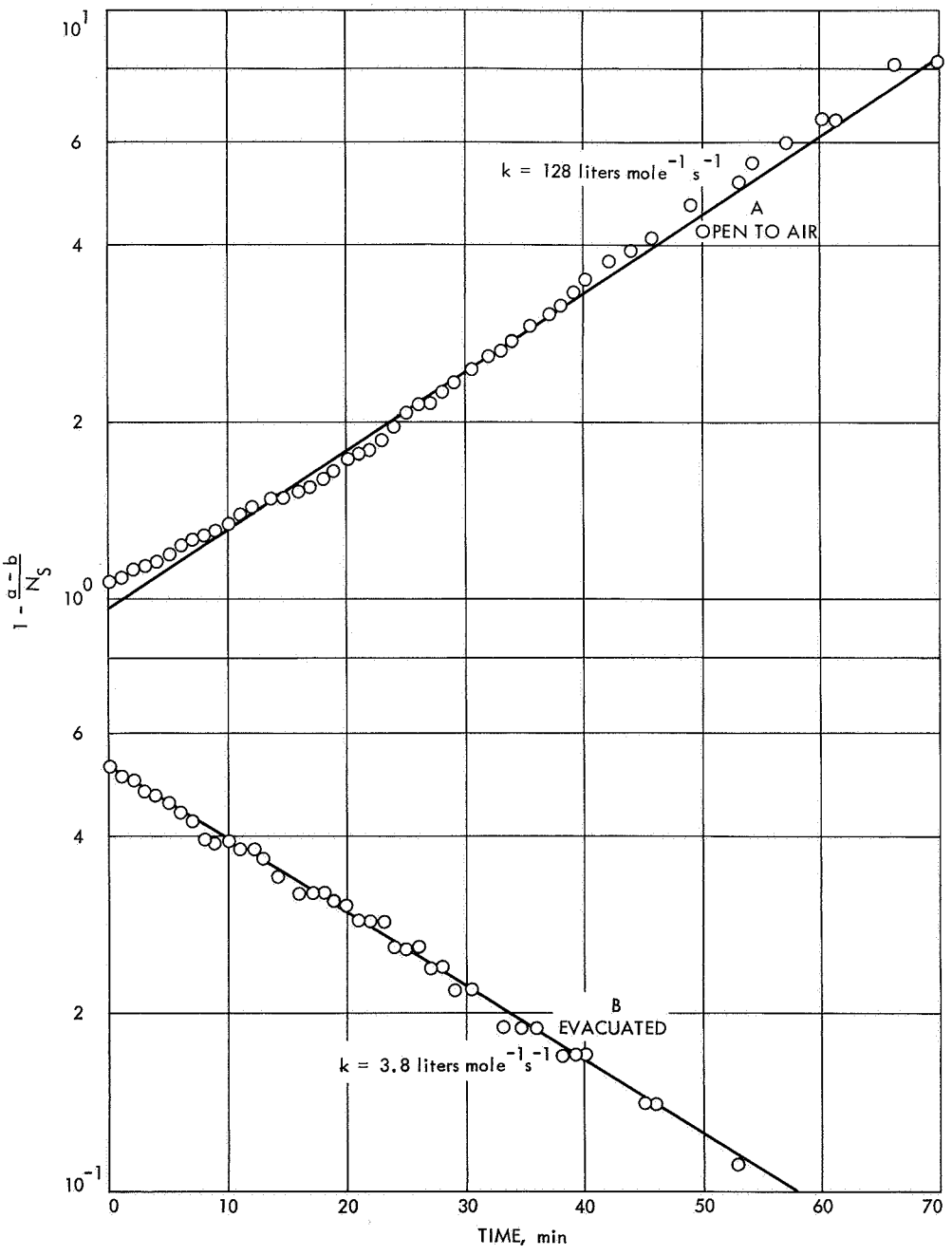

Fig. 6. Second-order decay of γ-irradiated crosslinking agent (Structure Fig. 1a at 110°C)

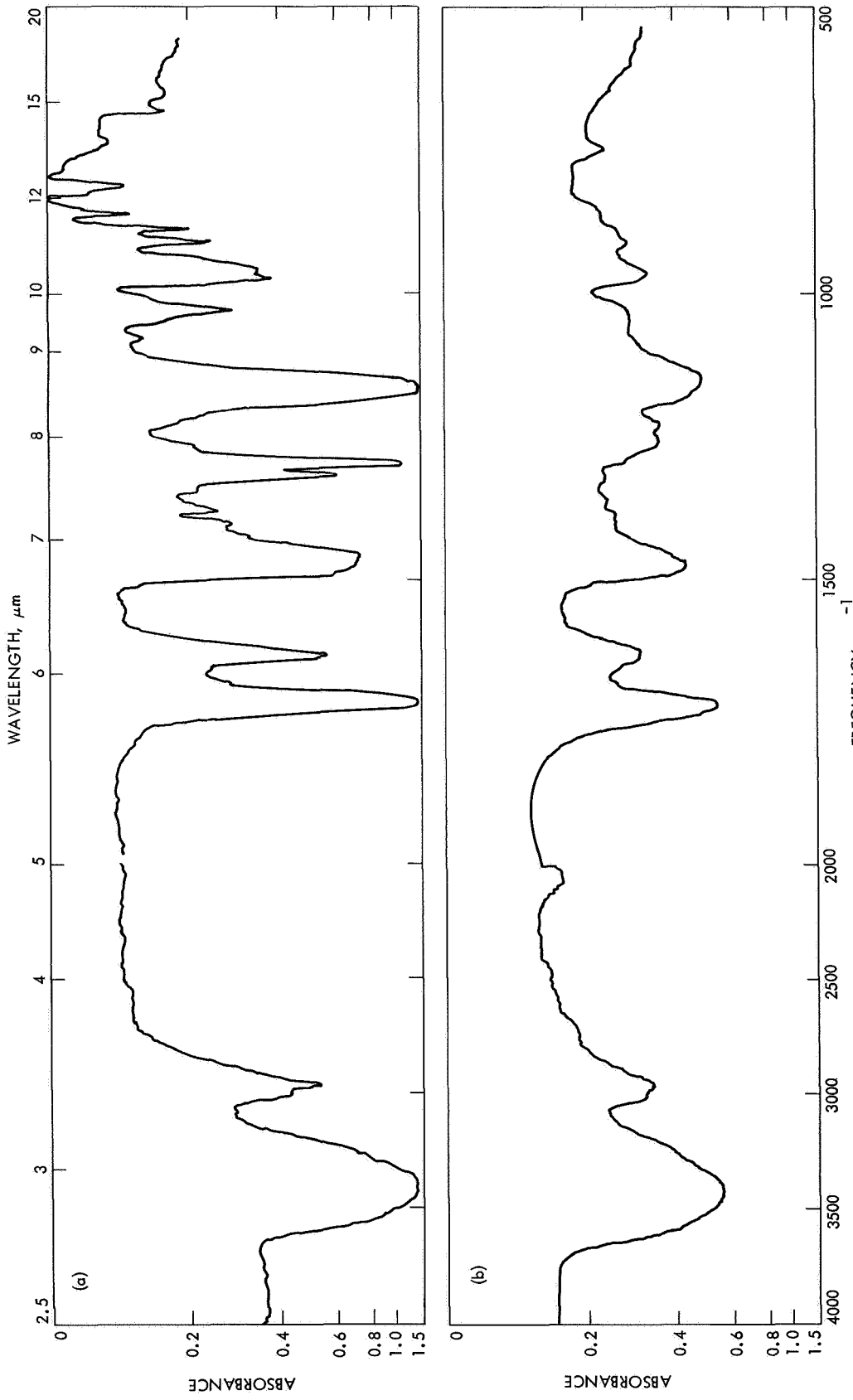

Fig. 7. IR spectra: (a) monomer (structure Fig. 1a) and (b) γ-irradiated polymer

the ESR spectrum (Fig. 4c) is interpreted as being due to a radical whose structure is

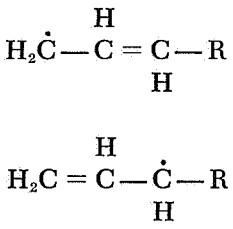

It is to be noted that the allyl radical formed by hydrogen abstraction is stabilized by resonance, a feature responsible for the lack of homopolymerization of the diallyl crosslinking agent.

The relative stability of these crosslinked polymers under cobalt radiation became apparent during this study. Solvent extraction and liquid gas chromatography showed an absence of volatile products after a 140-Mrad dose. The IR spectrum after this radiation treatment (Fig. 7) was identical to that obtained by redox polymerization of the monomer.

References

1. Daniels, F., *Physical Chemistry*, John Wiley & Sons, Inc., New York, 1948.
2. Fiścher, H., *J. Polymer Sci.*, Part B, Vol. 2, p. 529, 1964.
3. Symons, M. C. R., *J. Chem. Soc., (London)*, p. 1186, Feb. 1963.
4. Abraham, R. J., and Whiffen, D. H., *Trans. Faraday Soc.*, Vol. 54, p. 1291, 1958.
5. Fujimoto, M., and Ingram, D. J. E., *Trans. Faraday Soc.*, Vol. 54, p. 1304, 1958.

C. Evidence for Activated Carrier Mobility in Organic Solids, *F. Gutmann, A. M. Hermann, and A. Rembaum*

Steady-state space charge limited currents (SCLC) were obtained at different temperatures for a series of dipyridylium model compounds (Fig. 8) into which one TCNQ molecule (tetracyanoquinodimethane), in form of a radical ion, was introduced. Some compounds were produced containing two molecules of TCNQ, one associated with each ring. Polymers of these compounds were also produced and SCLC measured. The details of preparation will appear in a forthcoming issue of the *Journal of Physical Chemistry*.

The conductivity measurements were made on 0.5-in. diam cylindrical pellets. Pellets prepared under pressures

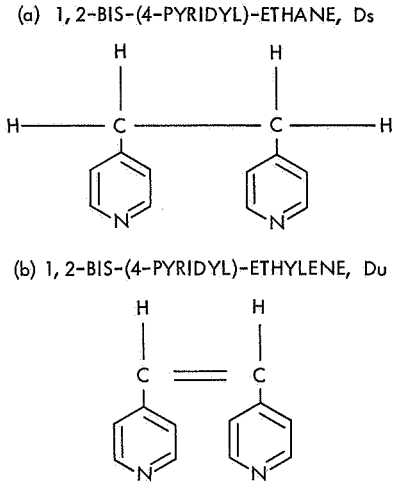

Fig. 8. Dipyridylium model compound chemical structure

in vacuum between 20,000 and 100,000 lb/in. had essentially identical conductivities. Electrical contact was made with vacuum-deposited gold electrodes or, in some cases, contacts were applied by covering the top and bottom surfaces with a thin layer of gold powder followed by recompression in the hydraulic press. Both processes resulted in firmly adherent, cohesive contacts ohmic at voltages below those at which appreciable charge injection occurred. In only one case was it possible to carry out measurements on a single crystal; the resulting activation energy (0.129 eV) is close to that obtained with the compactions (0.103 eV).

The conductance measurements were carried out in an evacuated glass cell (containing a thermocouple) immersed in a dewar vessel containing the temperature bath. Voltages up to 550 V were obtained from a Hewlett–Packard regulated power supply and those higher from a rectified power supply capable of delivering 5 mA. Currents and voltages were measured by means of Hewlett–Packard vacuum-tube voltmeters and Keithley electrometers.

The concentrations of free carriers at thermal equilibrium, n_{co}, were obtained (Ref. 1) from the transition voltage, V_{tr}, from ohmic to parabolic voltage dependence evaluated graphically using

$$n_{co} = \frac{2\epsilon\epsilon_0 V_{tr}}{et^2} \tag{1}$$

where e is the charge of the electron, ϵ_0 the permittivity of free space, ϵ the relative permittivity, and t is the inter-electrode spacing. With knowledge of the carrier concentration and the conductivity σ, the mobility may

then be obtained from

$$\mu = \frac{\sigma}{en_{co}}, \qquad \text{cm}^2/\text{V-s} \tag{2}$$

The results are summarized in Fig. 9. It is seen that the carrier concentration remains substantially constant to plus or minus an order of magnitude, at about 10^{11} cm^{-3}, over a temperature range in which the resistivities, some of which are also shown, change by up to eight orders of magnitude. In view of the uncertainties involved in the graphical location of V_{tr} and the probable changes in the effective permittivity at low temperatures, the values of n_{co} are estimated to be accurate only to within a factor of five. The largest apparent change in n_{co} was found in the unsaturated Du 1-TCNQ compound, which appeared to drop from 4.5×10^{11} at $-187°$C to 1.2×10^{10} at $-78°$C. In that temperature interval, the conductivity increased by five orders of magnitude.

While the temperature dependence of the mobility deduced from SCLC data could be fitted to a shallow-trap model (Ref. 2), this would require mobilities substantially larger than those shown in Fig. 9. These would

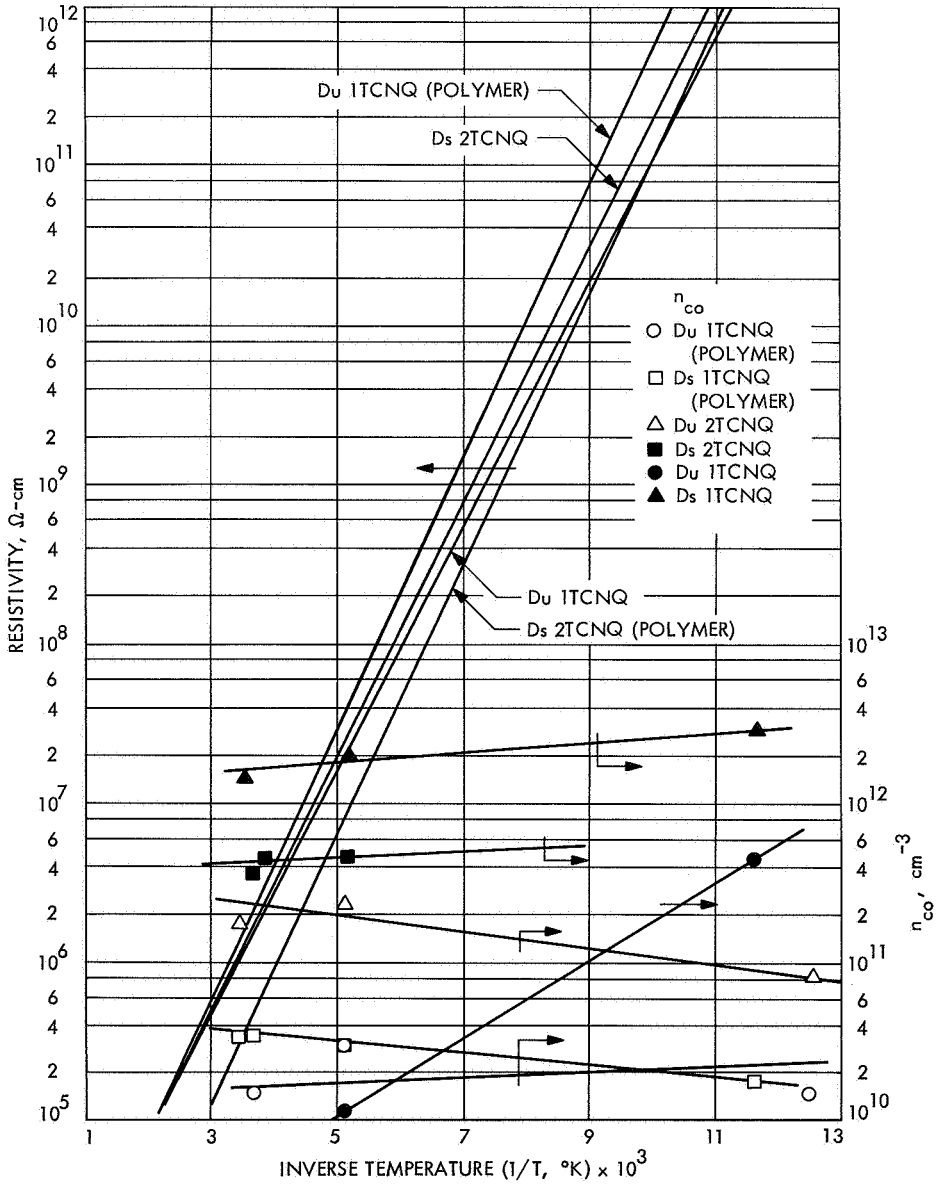

Fig. 9. Temperature dependence of resistivity (ρ) and concentration of carriers (n_{co})

not only be in greater discrepancy with Hall mobility measurements, but would require mobilities ($\gtrsim$ 40,000 cm²/V-s larger than those found in most single-crystal inorganic semiconductors; mobilities this large are extremely unlikely in systems lacking long-range order.

Thus, the conclusion is unavoidable that the observed conductivity changes are due to mobility changes. Such a thermally-activated mobility in organic materials has been proposed repeatedly (Refs. 3–8), but, to our knowledge, this work presents the first evidence for its existence.

It is of interest that, again to plus or minus an order of magnitude, the carrier concentration values appear to be invariant with respect to saturation versus unsaturation, introduction of a second TCNQ molecule, and polymerization. In fact, carrier concentration of the order discussed herein has also been observed by other researchers (Ref. 9).

References

1. Lampert, M. A., Rose, A., and Smith, R. W., *J. Phys. Chem. Solids*, Vol. 8, p. 464, 1959.
2. Rose, A., *Phys. Rev.*, Vol. 97, p. 1538, 1955.
3. Frolich, H., and Sewell, G. L., *Proc. Phys. Soc. London*, Vol. 74, p. 643, 1959.
4. Tredgold, R. H., *Proc. Phys. Soc. London*, Vol. 80, p. 807, 1962.
5. Pohl, H. A., and Opp, D. A., *J. Phys. Chem.*, Vol. 66, p. 2121, 1962.
6. Hadek, V., Ulbert, K., *Coll. Czech. Chem. Comm.*, Vol. 32, p. 1118, 1967.
7. Hermann, A. M., and Rembaum, A., *J. Polymer Sci.*, Part C, Vol. 17, p. 120, 1967.
8. Cherry, R. J., *Quart. Rev.*, Vol. 22, p. 162, 1968.
9. Gutmann, F., and Lyons, L. E., *Organic Semiconductors*, John Wiley & Sons, Inc., New York, 1967.

D. The Ethylene Oxide–Freon 12 Decontamination Procedure: The Control and the Determination of the Moisture Content of the Chamber,

R. H. Silver and S. H. Kalfayan

1. Introduction

The evaluation of several commercially available humidity sensing and controlling instruments for use in an ethylene oxide (ETO)–Freon 12 atmosphere was discussed in SPS 37-52, Vol. III, pp. 101–105. Instruments evaluated and discussed included the electrical-resistance, electrical-impedance, and optical–cold mirror types. None of the sensors were wholly satisfactory for service in the ETO–Freon 12 environment.

Since the last article, another optical–cold mirror type instrument was evaluated. The sensor of this instrument proved to be the most satisfactory tested so far. The results of these tests are described herein.

2. Experimental

The sensor of the test instrument, obtained from Cambridge Systems, Inc., is shown in Fig. 10. The general class of this type of humidity sensor is described in SPS 37-52, Vol. III, and Refs. 1 and 2.

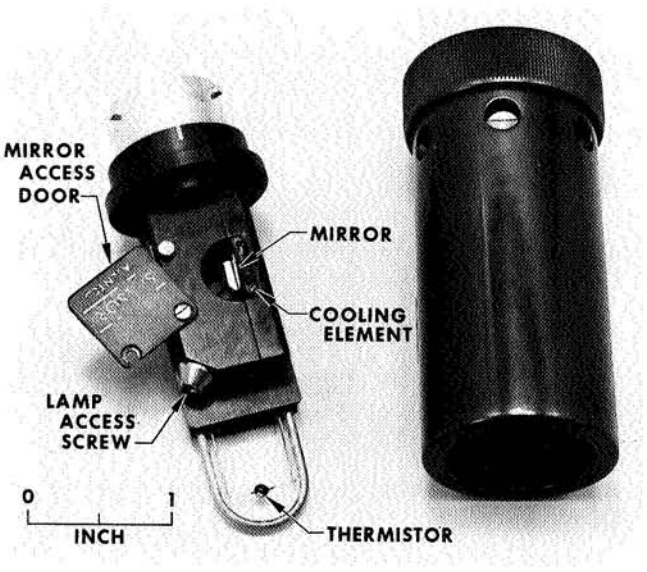

Fig. 10. Optical–cold mirror type sensor — Cambridge Systems, Inc., Model 137-S1-TH

The test procedure consisted of measuring the dew point in air at room conditions both before and after exposure of the sensing element to the ETO–Freon 12 decontamination chamber. Measurements were made simultaneously or within the minute. The computed percent relative humidity (RH) values were compared with those obtained by the manual dewpointer (Alnor Instrument Company, Model 7000 U), which served as a reference standard and is considered to be capable of measuring RH with an accuracy of $\pm 2\%$.

3. Results and Discussion

Because the reference standard is not suitable for use in the ETO–Freon 12 chamber, the desirable performance evaluation of the test instrument *in situ* could not be made. Consequently, the readings taken in air after the test sensor was exposed to ETO–Freon 12 were only a measure of the effects of the ETO–Freon 12 exposure

on the sensor. However, dew point or RH measurement in ETO–Freon 12 at the decontamination temperature of 50°C were made, and the results compared with those obtained by the electrical-resistance type hygrometer (SPS 37-52, Vol. III).

Table 3 gives the differences between the RH values obtained by the test sensor and the reference standard, $\Delta_{RH} = (RH_{test\ sensor} - RH_{standard})$. The Δ_{RH} values for the electrical-resistance type sensor are also included. The latter type is commonly used for RH determinations in the ETO decontamination chambers. The Δ_{RH} values obtained for the optical–cold mirror type sensor were low, indicating a close agreement with the readings of the reference standard. The Δ_{RH} values were generally positive. The Δ_{RH} values obtained for the electrical-resistance type sensor, except for the unexposed condition, were relatively high and consistently negative.

Table 3. Difference in RH values obtained by test sensors and reference standard

ETO–Freon 12 chamber exposure, h	Δ_{RH} electrical-resistance type sensor	Δ_{RH} optical–cold mirror type sensor	RH of air during measurements
0 (unexposed)	2.6 ± 1.4	1.6 ± 0.9	43.0 – 46.0
60	8.2 ± 0.6	1.0 ± 0.05	52.0 – 53.0
180	12.6 ± 0.8	1.3 ± 0.5	32.5 – 35.0
360	10.2 ± 0.01	1.3 ± 0.3	47.0

The percent RH readings from the electrical-resistance type sensor were 10–15 points lower than those from the optical–cold mirror type when both were placed in the ETO decontamination chamber operating at 50°C. Table 3 shows that this kind of difference in range was also obtained when readings were made in air, at room conditions, after exposure to ETO–Freon 12.

4. Conclusions

(1) The sensitivity of the optical–cold mirror type sensor was not impaired after long exposure to the ETO–Freon 12 environment.

(2) The relative humidity readings made by this instrument agreed closely with those made by the reference standard.

(3) The sensitivity of the electrical-resistance type sensor was changed by exposure to the ETO–Freon 12 atmosphere, and the RH readings thereafter were consistently lower by 8–13 points than those of the reference standard.

(4) There was no indication, however, that a continuous deterioration of the sensor took place by prolonged exposure to the ETO–Freon 12 decontamination atmosphere.

References

1. *General Catalog,* Cambridge Systems, Inc., Newton, Mass., 1968.
2. Paine, L. C., and Farrah, H. R., "Design and Application of High Performance Dewpoint Hygrometers," in *Humidity and Moisture, Vol. I,* pp. 174–188. Edited by A. Wexler, Reinhold Publishing Company, New York, 1965.

E. Dependence of Relative Volume on Strain for an SBR Vulcanizate, *R. F. Fedors and R. F. Landel*

1. Introduction

Although the importance of direct measurements of the volume change of an elastomer on stretching is readily recognized, very little data (especially at large strains) appear in the literature. The data that have been published are almost exclusively limited to either natural rubber gum vulcanizates cured with peroxides, which are known to undergo significant stress-induced crystallization at sufficiently high strains, or to noncrystallizable elastomers which, however, contained active fillers such as carbon black (Refs. 1–4).

Both the occurrence of crystallization and the presence of filler make at least some portions of the volume-extension response difficult to interpret. For example, L. Mullins and N. R. Tobin (Ref. 2) working at extension ratios of up to 5 find that for a natural rubber vulcanizate cured with peroxide, the relative volume first increases with strain, then passes through a very broad region containing a maximum, and finally goes through zero to become negative as the strain is further increased. Near the maximum, the volume increase due to the hydrostatic component of the stress becomes comparable to the volume decrease accompanying stress-induced crystallization.

Beyond the maximum, which for the data of Mullins and Tobin occurs at an extension ratio of about 3.5, the volume decrease due to crystallization swamps out the pure hydrostatic contribution. It is likely that crystallization occurs at extension ratios less than that at which the maximum appears, and a legitimate question to ask is: What is the strain interval for which stress-induced crystallization is negligible and hence can be safely ignored?

Since the hydrostatic component of stress gives rise to relative volume changes of the order of 10^{-4}, even small extents of crystallization can contribute significantly to the observed volume change. For example, assuming the density of the crystalline phase to be 0.97 g/cm³ and the density of the amorphous phase to be 0.91 g/cm³ (Ref. 5), only about 0.16% of the material would have to undergo stress-induced crystallization in order to produce a relative volume change (decrease) of 10^{-4}. Such small extents of crystallization would be difficult to detect, especially if the gross stress–strain behavior of the material were used as the sole criterion.

Using more sensitive X-ray methods, S. G. Nyburg (Ref. 6) reports, for a natural rubber-peroxide vulcanizate, a threshold extension ratio of about 3.5 below which no stress-induced crystallinity was observed. However, the usual X-ray determination of crystallinity is not particularly sensitive to very small extents of crystallization. Using low-angle light scattering, W. Yau and R. S. Stein (Ref. 7), working with a sulfur-cured natural rubber vulcanizate, report the presence of heterogenities that parallel the development of stress-induced crystallization at extension ratios of 2 to 3. This range is below the extension ratio at which crystallinity is first detected by X-rays.

A few years ago, volume–extension data were reported for a noncrystallizable styrene–butadiene copolymer (SBR) vulcanizate (SPS 37-18, Vol. IV, pp. 113–120) and, apparently, these still represent the only published data for such a system taken to large strains. Since the data were not fully discussed in the preliminary account, the purpose of this article is to more adequately describe and interpret the significance of the data.

2. Experimental Part

a. Material and characterization. The material studied was a gum vulcanizate based on a noncrystallizable SBR-1500. The gum contained 0.5 parts of dicumyl peroxide per 100 parts of rubber and was vulcanized for 0.5 h at 150°C. The measured density is 0.951 g/cm³. The stress–strain response in uniaxial tension was measured at 25°C on a ring-shaped specimen at a strain rate of 1.16/min. These data, represented by the filled circles, are shown in Fig. 11 as a plot of the stress as a function of the extension ratio.

In an attempt to find an analytic form for these stress–strain results, several of the more commonly used one- and two-parameter stress–strain relationships were evaluated. As might be anticipated, the two-parameter expressions were superior to those containing only one parameter.

The dashed curve shown in Fig. 11 is the fit provided by the two-parameter Mooney–Rivlin equation (Refs. 8 and 9) which has the form

$$\sigma = \left(\lambda - \frac{1}{\lambda^2}\right)\left(2C_1 + \frac{2C_2}{\lambda}\right) \tag{1}$$

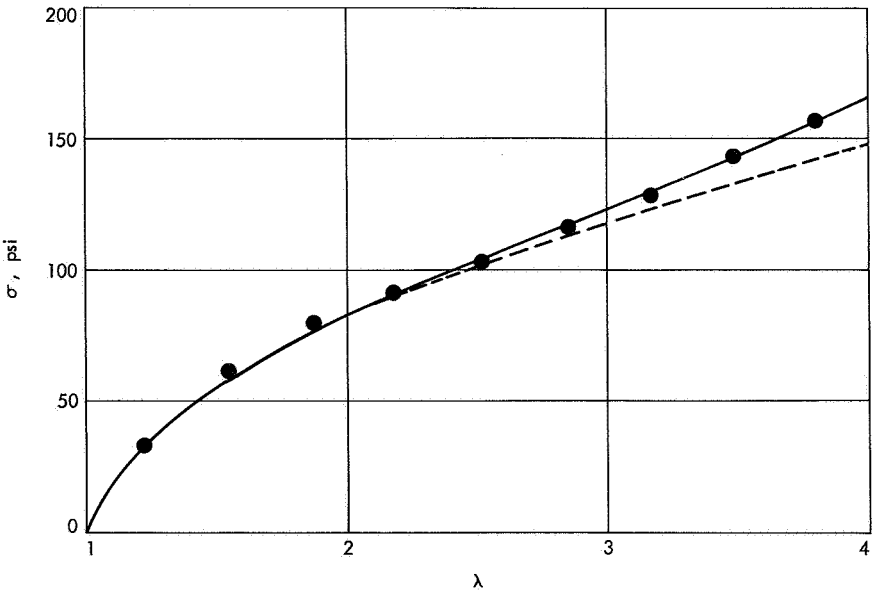

Fig. 11. Stress–strain response for an SBR peroxide vulcanizate

where σ is the stress based on the original cross-sectional area, λ is the extension ratio, and $2C_1$ and $2C_2$ are constants. For the fit shown, $2C_1 = 28$ psi and $2C_2 = 38$ psi. It is evident that Eq. (1) provides a good fit to the experimental data at least for λ values up to about 3. For larger λ, the experimental data fall above the response predicted by Eq. (1).

The solid curve shown in Fig. 11 is the fit provided by the Martin–Roth–Stiehler (MRS) equation (Ref. 10) which has the form

$$\sigma = E\left(\frac{1}{\lambda} - \frac{1}{\lambda^2}\right)\exp\left[A\left(\lambda - \frac{1}{\lambda}\right)\right] \qquad (2)$$

where E is Young's modulus and A is a parameter that depends on both the degree of crosslinking and the time scale. For the fit shown, $E = 174$ psi and $A = 0.43$. As can be seen, this expression provides a good representation for the experimental data over the entire range of λ. Thus, for the present data, the MRS equation provides a better fit than does the Mooney–Rivlin equation.

b. Volume changes on extension. The relative volume changes on extension are of the order of 10^{-4} and, hence, too small to be determined accurately by any simple technique that relies on measurement of linear specimen dimensions. Therefore, a direct measure of the volume change itself is preferred and simple hydrostatic weighing was employed. A rig was made up similar to that employed by Mullins and Tobin whereby four ring specimens 1.375-in. ID × 1.625-in. OD and about 0.1-in. thick could be stretched under water in 0.5-in. increments. The totally-immersed rig and either relaxed or extended specimens were suspended by a 10-mil platinum wire from a Mettler single-arm analytical balance mounted on an essentially vibration-proof table. The water temperature was maintained at 23 ±0.05°C.

Since rubber vulcanizates absorb water to some extent, the specimens were relaxed and reweighed between each successively increasing strain increment in order to follow the absorption of water. The results are shown in Fig. 12 where the weight of the immersed rig and specimens is shown as a function of the immersion time and extension ratio. After about 50 min, the immersed weight of the relaxed specimens increased essentially linearly with time. The rate of increase in weight was 7.72×10^{-5} g H_2O/min which corresponds to a rate of 1.93×10^{-5} g H_2O/g rubber/h for specimens with a surface-to-volume ratio of about 14 cm^{-1}.

Ideally, one would like to have a system in which the relaxed specimens undergo no weight change with time. The rate of change in weight can be reduced by using more rubber, especially if the surface-to-volume ratio is also decreased. At the conclusion of the run, i.e., after about 150 min, the water adhering to the surface of the broken rings was removed by blotting and the weight of the rings in air was measured. The difference between the

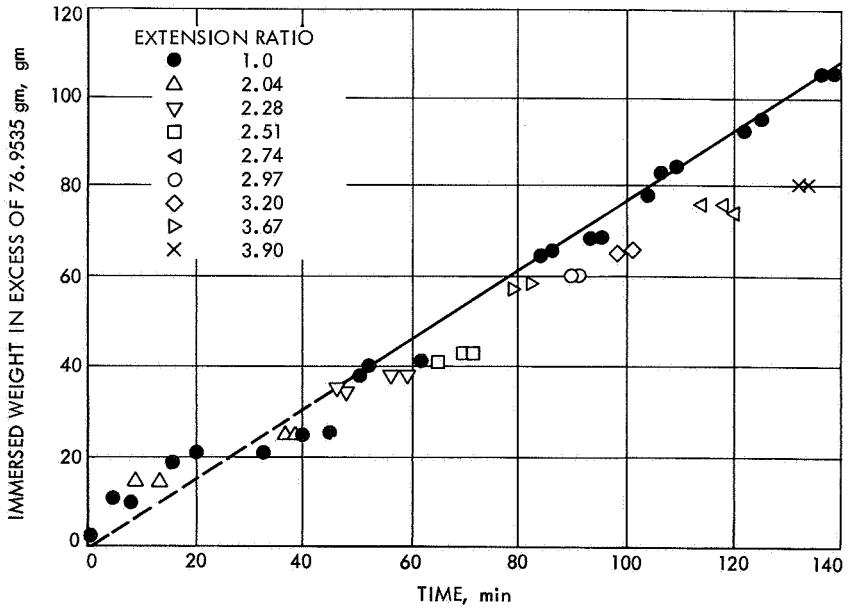

Fig. 12. Immersed weight of rig and specimens as a function of time

final and initial weight in air yields a value of 0.0124 g for the weight increase. This corresponds to a water pickup of 3.10×10^{-3} g H_2O/g rubber if it is assumed that the weight change is due solely to water absorption. The volume of water absorbed by the specimens thus exceeds by about an order of magnitude the relative volume change expected to be produced by the hydrostatic component of stress.

The change in weight on extension was taken as the difference in weight of the extended specimens and the weight of the relaxed specimens, the latter as interpolated from the linear portion of the curve. The data for times less than about 50 min were not used.

The average value of the relative volume change, $\Delta V/V_0$, as a function of the extension ratio is shown in Fig. 13 as the filled circles. The length of the bar associated with each point represents the scatter observed for $\Delta V/V_0$. The scatter appears to be typical of this type of measurement and is comparable to that reported by F. G. Hewitt and R. L. Anthony (Ref. 3). The solid curve shown in Fig. 13 represents the prediction of Eq. (14) using the experimental stress–strain curve.

3. Discussion

In this subsection, it will be pointed out that, for the present SBR vulcanizate, the observed increase in weight of the relaxed specimens with time, as indicated in Fig. 12, can be simply interpreted as due to water entering and filling up voids and cavities pre-existing in the rubber without, at the same time, causing the volume to increase. That is, the specimen volume is constant and

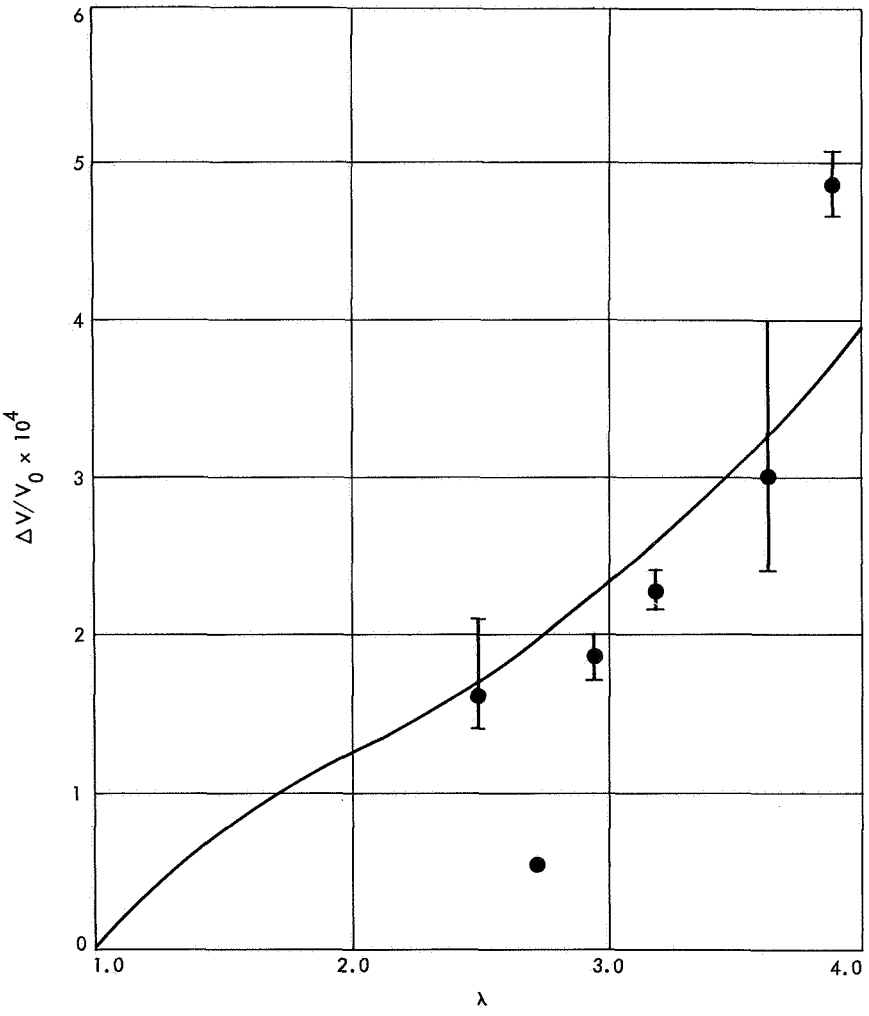

Fig. 13. Dependence of relative volume increase on extension ratio

independent of time. Considering this to be the primary cause of the observed weight increase with time, a simple argument will show that the deformation of these cavities will not contribute an appreciable component to the volume–extension response.

a. Water absorption. The immersed weight of the rig and specimens as a function of time can be written as

$$W_{imm} = V_{rig}(\rho_{rig} - \rho_w) + V_{ru}(t)[\rho_{ru}(t) - \rho_w] \quad (3)$$

where V_{rig} and ρ_{rig} are the volume and density of the rig, respectively; $V_{ru}(t)$ and $\rho_{ru}(t)$ are the time dependent volume and density of the specimens, respectively; and p_w is the density of water. The equation assumes that the observed time dependence is due entirely to the effect of water on the rubber.

The rate of change of the immersed weight with time can be obtained from Eq. (3) as

$$\frac{dW_{imm}}{dt} = \frac{dV_{ru}(t)}{dt}[\rho_{ru}(t) - \rho_w] + V_{ru}(t)\frac{d\rho_{ru}(t)}{dt} \quad (4)$$

Various assumptions concerning the effect of water absorption on both $V_{ru}(t)$ and $\rho_{ru}(t)$ can now be made in order to determine which model most closely predicts the experimental data of Fig. 12.

For example, if we assume that the absorbed water increases both the specimen weight and volume, and further that the total volume is the sum of the volume of rubber and absorbed water, then it is easy to show that

$$V_{ru}(t) = V_{ru}(0)\left[\frac{\rho_w + x(t)\rho_{ru}(0)}{\rho_w}\right] \quad (5)$$

where $x(t)$ is the weight fraction of water absorbed at time t. Similarly, the density can be written as

$$\rho_{ru}(t) = \frac{\rho_w\rho_{ru}(0)[1 + x(t)]}{\rho_w + x(t)\rho_{ru}(0)} \quad (6)$$

Substituting Eqs. (5) and (6) into Eq. (4) yields the result $dW_{imm}/dt = 0$. Thus, the assumption that the absorbed water merely increases the volume of the rubber by simple additivity leads to the prediction that the immersed weight will be time independent. The data in Fig. 12 show that this assumption must be rejected.

On the other hand, we can assume that the absorbed water increases the weight of the specimen without producing any concomitant volume change. This assumption would imply that the water fills up pre-existing voids and cavities present in the rubber. The following expressions are easily derived:

$$V_{ru}(t) = V_{ru}(0) \quad (7)$$

and

$$\rho_{ru}(t) = \rho_{ru}(0)[1 + x(t)] \quad (8)$$

Substituting Eqs. (7) and (8) into Eq. (4), we obtain

$$\frac{dW_{imm}}{dt} = V_{ru}(0)\rho_{ru}(0)\frac{dx}{dt} \quad (9)$$

Since x is an increasing function of time, Eq. (9) predicts a positive slope for dW_{imm}/dt. Also, since the slope in Fig. 12 is constant, x is a linear function of time: $x = 1.93 \times 10^{-5}t$. Knowing $x(t)$ explicitly as well as the duration of the run, we can now calculate the total water absorption and compare it to the measured value which is 3.10×10^{-3} g H_2O/g rubber. The value predicted using $x = 1.93 \times 10^{-5}t$ is 2.90×10^{-3} g H_2O/g rubber. Thus, the close correspondence between the predicted and measured water absorption lends support to the notion that water fills pre-existing voids and cavities.

An alternative way to explain the data of Fig. 12 is to assume that the water leaches out water-soluble materials, present in the rubber, whose density is less than that of water. The water can then replace the material lost. The difference between the two approaches thus relates to whether the voids and cavities pre-exist in the rubber or are formed by a leaching-out process. Unfortunately, the *dried* weight of the specimens was not measured after the test and so it is not known if any material was leached out during the run.

b. Effect of deformation of cavities on volume change. If the absorbed water is indeed present in the form of filled cavities, it is easy to demonstrate that the deformation of such cavities will not contribute appreciably to the volume–strain response. For simplicity, assume that the water present fills a single spherical cavity. Uniaxial deformation of the rubber will deform the sphere into a prolate spheroid. Further, since the water present can easily accommodate a deformation, no dewetting in the sense of a separation of the rubber from the water should occur. If V_w is the volume of water present per cubic

centimeter of rubber, then the relationship between V_w and the radius, r_0, of the spherical cavity is

$$V_w = \frac{4}{3}\pi r_0^3 \tag{10}$$

As the specimen is deformed to an extension ratio λ_1, the major radius of the deformed sphere, r_1, will be $r_1 = \lambda_1 r_0$. The minor radii r_2 and r_3 will be equal and will be taken as $r_2 = \lambda_2 r_0$. Since

$$\lambda_1\lambda_2^2 = [1 + (\Delta V/V_0)]$$

the minor radius is

$$r_2 = \frac{r_0\left(1 + \frac{\Delta V}{V_0}\right)^{1/2}}{\lambda_1^{1/2}} \tag{11}$$

The volume of the deformed sphere is

$$\frac{4}{3}\pi r_0^3\left(1 + \frac{\Delta V}{V_0}\right) \tag{12}$$

while the volume of the original sphere is $(4/3)\pi r_0^3$. Thus, the relative volume change contributed by the deformation of the sphere alone is $V_w(\Delta V/V_0)$. Since V_w was measured to be 2.95×10^{-3} cm^3 H_2O/cm^3 rubber, it is obvious that we can neglect volume changes attending deformation of the cavity. The water was assumed to be present in a single spherical cavity; however, variation in the number of cavities or in the shape should not alter significantly the results obtained on the assumption of a single sphere.

c. Temperature effects. The water bath employed for hydrostatic weighing was maintained at a constant temperature to within about 0.1°C. It is, therefore, important to know the effect of such a temperature variation on the observed weight data. It is easy to demonstrate that the change in weight accompanying a temperature change of ΔT is given by

$$\Delta W_{imm} = \frac{\rho_w \Delta T}{1 + \beta_w \Delta T}\left[V_{rig}(\beta_w - \beta_{rig}) + V_{ru}(\beta_w + \beta_{ru})\right] \tag{13}$$

where β_w, β_{rig}, and β_{ru} are the cubical expansion coefficients of water, rig, and specimens, respectively. The change in immersed weight is

$$\Delta W_{imm} \approx 0.1\left[11.4\,(1.6 \times 10^{-4}) - 4.2\,(4 \times 10^{-4})\right]$$

where

$$\Delta T = 0.1°\text{C}$$

$$\beta_w = 2 \times 10^{-4}$$

$$\beta_{rig} = 0.4 \times 10^{-4}$$

$$\beta_{ru} = 6 \times 10^{-4}$$

$$V_{rig} = 11.4\ \text{cm}^3$$

$$V_{ru} = 4.2\ \text{cm}^3$$

or

$$\Delta W_{imm} \approx 1.4 \times 10^{-5}\ \text{g}$$

and, hence, weight changes caused by temperature fluctuations of about 0.1°C can be ignored.

d. Form of the volume–strain response. Several expressions have been proposed to relate volume change to extension. For example, based on thermodynamic arguments, G. Gee (Ref. 1) derived the expression

$$\frac{\Delta V}{V_0} = \frac{1}{3B}\int_1^{\lambda} \lambda\left(\frac{\partial \sigma}{\partial \lambda}\right)d\lambda \tag{14}$$

where B is the bulk modulus. This expression assumes the material to remain isotropic in the stretched state. If the actual stress–strain curve were at hand, or if an explicit analytic form were available, Eq. (14) could be employed to predict the volume–extension response. It is of interest to consider how the volume–extension response depends on the form of the stress–strain response.

One-parameter equation. If it is assumed that the kinetic theory expression is an adequate representation of the stress–strain response, then Eq. (14) can be integrated directly to yield

$$\frac{\Delta V}{V_0} = \frac{E}{9B}\left[\frac{\lambda^2 - 1}{2} + 2\left(1 - \frac{1}{\lambda}\right)\right] \tag{15}$$

This expression was shown by Hewitt and Anthony to be in good accord with their experimental volume–strain response for λ values up to about 1.5. However, this approach presents some conceptual difficulties, for the kinetic theory expression is derived under the restriction that there is *no* volume change on stretching. The apparent contradiction is resolved by assuming that the

volume change makes such a negligibly small contribution to the stress–strain curve that the kinetic theory expression is still adequate.

Another one-parameter stress–strain relationship of interest was proposed by G. M. Bartenev (Ref. 11), who established that the stress based on the deformed cross-sectional area is proportional to strain for strains up to 100–200%. This has been confirmed by T. L. Smith (Ref. 12) who finds, however, that deviations from strict linearity occur at strains of about 100%. Hence, assuming the stress strain response to be

$$\sigma\lambda = E\,\epsilon \tag{16}$$

the volume–strain response predicted by Eq. (14) becomes

$$\frac{\Delta V}{V_0} = \frac{E}{3B}\ln\lambda \tag{17}$$

It is noteworthy that a similar equation was found by Smith (Ref. 13) to afford a good representation to the volume–strain behavior of polyvinyl chloride glass bead composites.

An additional one-parameter expression that seems to have wide applicability was proposed by K. Valanis and R. F. Landel (Ref. 14):

$$\sigma = \frac{2}{3}\,E(\ln\lambda)\left(1 + \frac{1}{2\lambda^{3/2}}\right) \tag{18}$$

This equation was shown to provide a very good fit to both uniaxial *and* biaxial stress–strain data for λ in the range $1 < \lambda < 2$. In addition, Eq. (18) reproduces the general form of the stress–strain behavior of a Mooney–Rivlin material. Using Eq. (18), Gee's expression yields

$$\frac{\Delta V}{V_0} = \frac{2E}{9B}\left[\left(\lambda + \frac{2}{\lambda^{1/2}}\right) + \frac{3}{2}\,\frac{\ln\lambda}{\lambda^{1/2}} - 3\right] \tag{19}$$

Two-parameter equations. Perhaps the simplest of the two-parameter equations is the Mooney–Rivlin form. As might be expected, this generally provides a better representation of the observed stress–strain response than the one-parameter equation. Substituting Eq. (1) into Eq. (14), the volume–strain response for a Mooney–Rivlin material is

$$\frac{\Delta V}{V_0} = \frac{2C_1}{3B}\left[\frac{\lambda^2}{2} - \frac{2}{\lambda} - \frac{3}{2}\,\frac{C_2}{C_1\lambda} + \frac{3}{2}\left(1 + \frac{C_2}{C_1}\right)\right] \tag{20}$$

On the other hand, if the MRS relationship (Eq. 2) is substituted into Eq. (14), the resulting volume–extension response is not obtained in closed form, i.e., the following integral equation is obtained:

$$\frac{\Delta V}{V_0} = \frac{E}{3B}\int_1^\lambda \frac{[A\lambda^3 - (A+1)\lambda^2 + (A+2)\,\lambda - A]}{\lambda^4} \times \exp\left[A\left(\lambda - \frac{1}{\lambda}\right)\right]d\lambda \tag{21}$$

Once the value of A has been determined, the integral can be evaluated numerically.

Equations for the volume–extension response based on the use of Eq. (14), which have been derived above, implicitly assume that rubber remains isotropic in the stretched state. It was pointed out by T. N. Khasanovich (Ref. 15) that an elastomer would not be expected to remain isotropic at large strains, and, hence, that the integrand in Eq. (14) should be multiplied by a factor μ that takes into account the anisotropy of linear compressibility for a stretched material. If the elastomer obeys the kinetic theory stress–strain law derived by James and Guth, then Khasanovich shows that

$$\mu = \frac{3}{(\lambda^3 + 2)} \tag{22}$$

Using this result, Eq. (14) becomes

$$\frac{\Delta V}{V_0} = \frac{E}{3B}\left(1 - \frac{1}{\lambda}\right) \tag{23}$$

Figure 14 shows a comparison of the form of several of the $\Delta V/V_0$, λ expressions using the reduced relative volume change, $(\Delta V/V_0)\,(3B/E)$, as the variable on the ordinate. Curve 1 corresponds to the kinetic theory expression (Eq. 15); curve 2 corresponds to the Valanis–Landel expression (Eq. 19); curve 3 corresponds to the prediction of Eq. (14) obtained by actual integration of the experimentally obtained stress–strain curve taking B as 3.1×10^5 psi (a value close to that reported in the literature). This same curve also corresponds to the MRS expression (Eq. 21), using $E = 174$ psi and $A = 0.43$. Curve 4 corresponds to the Bartenev expression (Eq. 17); curve 5 corresponds to the Mooney–Rivlin expression (Eq. 20), using $2C_1 = 28$ psi and $2C_2 = 38$ psi; and curve 6 corresponds to the Khasanovich expression (Eq.

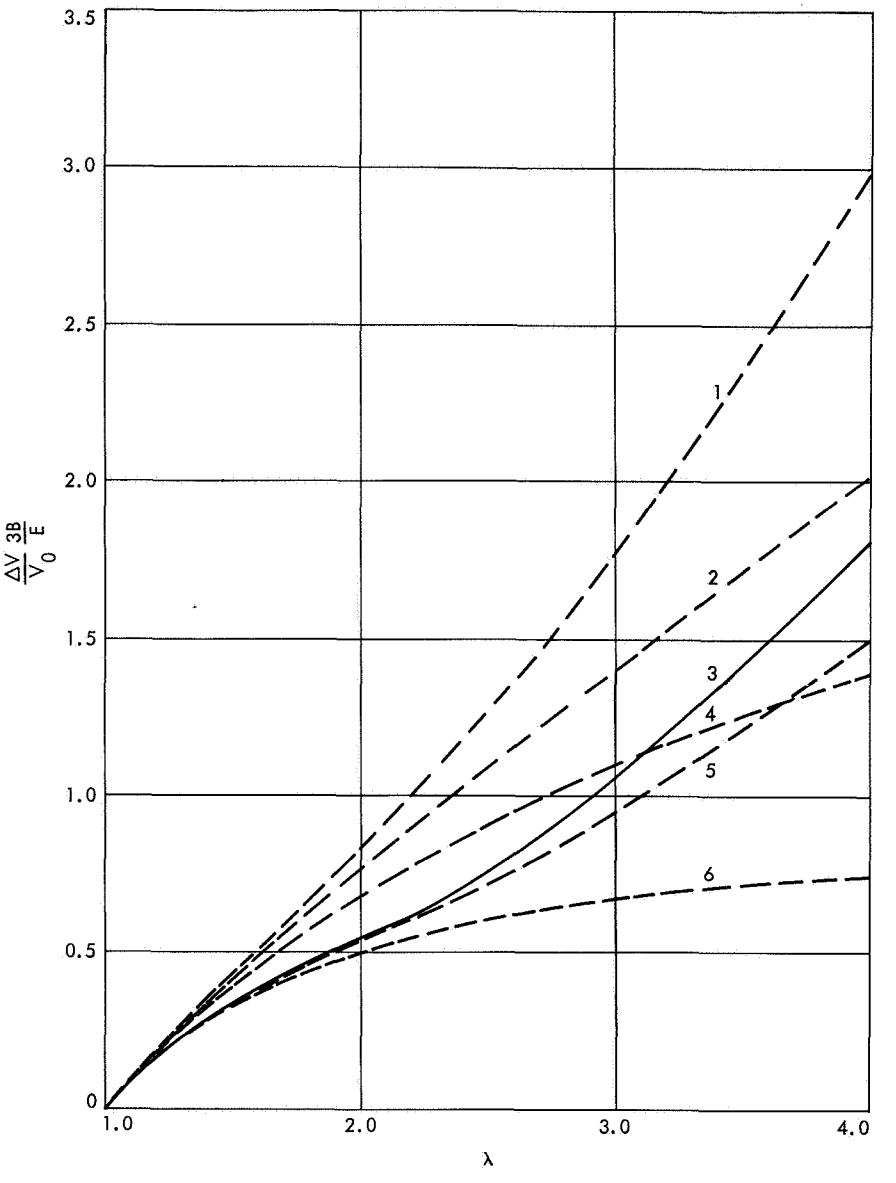

Fig. 14. Dependence of reduced relative volume increase on extension ratio

23). Of the various expressions considered, the upper limit to $\Delta V/V_0$ is apparently predicted by the kinetic theory expression, while the lower limit to $\Delta V/V_0$ is provided by the equation proposed by Khasanovich.

Figure 14 clearly demonstrates that, for small λ values, the predictions of the various proposals rapidly converge, so that, in this region, it will be difficult if not impossible to determine the degree of conformance to a given expression, especially in view of the scatter typical of $\Delta V/V_0$, λ data. At large strains, however, the predictions diverge so that it would be much easier to test for conformance in this region.

In Fig. 13, the solid curve corresponds to the predicted $\Delta V/V_0$, λ response using Gee's Eq. (14) with the integrated form of the experimental stress–strain curve. [This same curve is generated using the MRS expression (Eq. 21)]. The fit shown is considered satisfactory in view of the preliminary nature of these direct volume change measurements.

References

1. Gee, G., Stern, J., and Treloar, L. R. G., *Trans. Faraday Soc.*, Vol. 46, p. 1101, 1950.
2. Mullins, L., and Tobin, N. R., *Trans. Inst. Rubber Ind.*, Vol. 33, p. 2, 1957.

3. Hewitt, F. G., and Anthony, R. L., *J. Appl. Phys.*, Vol. 29, p. 1411, 1958.

4. Allen, G., Bianchi, U., and Price, C., *Trans. Faraday Soc.*, Vol. 59, p. 2493, 1963.

5. Miller, R. L., *Polymer Handbook*, p. 111-1. Edited by J. Brandrup, and E. H. Immergut. Interscience Publishers division of John Wiley & Sons, Inc., New York, 1966.

6. Nyburg, S. C., *Brit. J. Appl. Phys.*, Vol. 5, p. 321, 1954.

7. Yau, W., and Stein, R. S., *Polym. Lett.*, Vol. 1, p. 231, 1964.

8. Mooney, M., *J. Appl. Phys.*, Vol. 11, p. 582, 1940.

9. Rivlin, R. S., *Phil. Trans.*, Vol. A240, p. 459, 1948.

10. Martin, G. M., Roth, F. L., and Stiehler, R. D., *Trans. Inst. Rubber Ind.*, Vol. 32, p. 189, 1956.

11. Bartenev, G. M., *Kolloidn Zh.*, Vol. 11, p. 2, 1949.

12. Smith, T. L., *Trans. Soc. Rheol.*, Vol. 6, p. 61, 1962.

13. Smith, T. L., *Trans. Soc. Rheol.*, Vol. 3, p. 113, 1959.

14. Valanis, K., and Landel, R. F., *J. Appl. Phys.*, Vol. 38, p. 2997, 1968.

15. Khasanovich, T. N., *J. Appl. Phys.*, Vol. 30, p. 948, 1959.